micromachines

MDPI

Article

Labeling on a chip of cellular fibronectin and matrix metallopeptidase-9 in human serum

Briliant Adhi Prabowo [1], Carole Sousa [1], Susana Cardoso [2], Paulo Freitas *[1] and Elisabete Fernandes [1,*]

[1]International Iberian Nanotechnology Laboratory (INL), Braga, Portugal;
BAP: briliant.prabowo@inl.int; CS: carole.sousa@inl.int; PF: paulo.freitas@inl.int; EF: elisabete.fernandes@inl.int
[2]INESC-MN–Instituto de Engenharia de Sistemas e Computadores-Microsistemas e Nanotecnologias Lisboa, Portugal; SC: scardoso@inesc-mn.pt
* Correspondence: authors: paulo.freitas@inl.int and elisabete.fernandes@inl.int

Citation: Prabowo, BA.; Sousa, C.; Cardoso, S.; Freitas, P.; Fernandes, E, Labeling on a chip for human serum protein biomarkers *Micromachines* **2022**, x, x. https://doi.org/10.3390/xxxxx

Academic Editor: Firstname Lastname

Received: date
Accepted: date
Published: date

Abstract: We present a microfluidic chip for protein labeling in the human serum-based matrix. Serum is a complex sample matrix that contains a variety of proteins, and a matrix used in many clinical tests. In this work, the device performance was tested using commercial serum samples from healthy donors (commercial) spiked with the following target proteins: cellular fibronectin (c-Fn) and matrix metallopeptidase 9 (MMP9).The microfluidic molds were fabricated using micro milling on acrylic and using stereolithography (SLA) three-dimensional (3D) printing for an alternative method and comparison. Simple quality control was performed for both fabrication mold methods to inspect the channel height of the chip that plays a critical role in the labeling process. The fabricated microfluidic chip shows good reproducibility and repeatability of the performance for the optimized channel height of 150 μm. The spiked protein of cellular fibronectin (c-Fn) and matrix metallopeptidase 9 (MMP9) in the human serum-based matrix were successfully labeled by functionalized magnetic nanoparticles (MNPs). The biomarker labeling occurring in serum was compared using a simple matrix sample: phosphate buffer. The measured signals obtained by using a magnetoresistive (MR) biochip platform showed that the labeling using the proposed microfluidic chip is in good agreement for both matrixes, i.e., the analytical performance (sensitivity) obtained with serum, near the relevant cutoff values, is within the uncertainty of the measurements obtained with a simple and more controlled matrix: phosphate buffer. This finding is promising for stroke patient stratification where these biomarkers are found at high concentrations in serum.

Keywords: microfluidic chip; cellular fibronectin; MMP9; serum; magnetic nanoparticle; magnetoresistive; biosensor

1. Introduction

Detecting specific biomarkers in physiological body fluids, such as blood, serum, plasma, sweat, and urine is a challenge in the development of biosensors [1–4]. Even more, highlighted when the sample preparation takes a considerable amount of time and decreases the diagnostic tool's effectiveness. Analytical parameters such as selectivity and specificity are a further challenge for low concentrations of biomarkers. For example, in emergency medicine, the stratification of ischemic stroke patients should occur in the shortest time possible, because of the narrow time window for thrombolytic therapy [5–8]. Nevertheless, human blood is a complex sample matrix that can difficult access to relevant stroke biomarkers, such as cellular fibronectin (c-Fn) and matrix metallopeptidase 9 (MMP9) [6,9,10] – strongly associated with ischemic stroke screening in clinical studies for more than five decades [11,12]. When the obstacles to sample matrix complexity cannot be overcome, a sample preparation method preceding the detection is needed [3,13].

Microfluidics sparks much attention from scientists in sample pre-treatment, such as sample preparation devices for complex biological matrices, particle sorters, labeling processes, mixers, and flow manipulation from liquid mediums [13–20]. The conventional fabrication of microfluidic devices uses the casting polymer method on a mold as a master pattern that is fabricated using a costly lithography process[2]. Low-cost fabrication molds were introduced using micro-milling to engrave acrylic materials, simplifying the laborious lithography process and significantly cutting the fabrication cost [21,22]. Besides the straightforward fabrication process that can be done outside the cleanroom facilities, acrylic is an incredibly cheap material, transparent and robust for the master pattern of microfluidics, with a resolution down to 100 μm[21,23]. Nevertheless, reproducibility and low throughput yield are still the main issues of the micro-milling fabrication method.

The 3D printing process offers better reproducibility and high throughput production of the microstructure for microfluidics[24,25]. Several methods for 3D printing techniques, such as selective laser sintering, extrusion method, inkjet printing, and stereolithography (SLA), offer a broad spectrum in terms of cost, resolution, roughness, stiffness, and additive materials[26–28].

Herein, we demonstrate and compare the reproducibility and repeatability of a microfluidic chip for magnetic labeling of protein biomarkers using molds fabricated using micro-milling [29] and 3D printing with simple quality control. For that, we used two relevant stroke biomarkers, c-Fn, and MMP9. According to the literature, the simultaneous detection of these biomarkers can provide 87% prediction specificity for HT risk (the main side-effect of thrombolytic treatment in acute cases of stroke) [30]. To our knowledge, the development of a microfluidic chip for magnetic labeling of relevant stroke biomarkers using a human serum-based matrix is firstly presented. Moreover, the performance is compared when labeling occurs in a simple matrix: phosphate buffer. For the quantification of biomarkers was used a magnetoresistive (MR) biochip platform that validates the performance of the target labeling of c-Fn and MMP9 occurring on the MF chip.

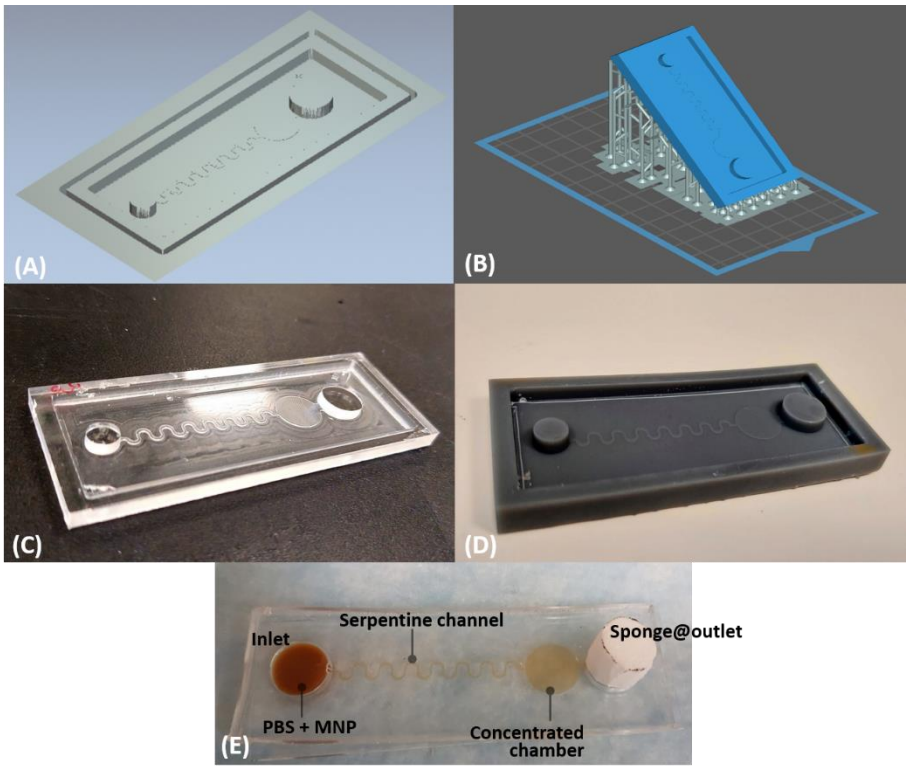

Figure 1. (A) Simulated micro-milling fabrication of the microfluidic mold in acrylic. (B) 3D model of the mold with 45° printing orientation using raft support. Fabricated mold using (C) micro-milling and (D) SLA 3D printing. (E) Fabricated microfluidic chip for test flow. The dimension of the microfluidic chip: total length = 75 mm; width = 25 mm; diameter of inlet = 7.5 mm, diameter of concentrated chamber and outlet = 10 mm; height of inlet and outlet = 3 mm; height of channel and concentrated chamber = 250 μm; width of serpentine channel = 250 μm; total length of serpentine channel = 88 mm.

2. Materials and Methods

2.1. Microfluidics mold fabrications

Microfluidic designs were drawn using AutoCAD 2013 (Autodesk Inc., USA). Next, the design will be fabricated both using micro-milling and SLA 3D printing. The mold fabrication using micro-milling computer numerical control (CNC) is simulated using ArtCAM software for mapping the sequence of engraving and cutting (Fig. 1A), the process is described in detail in [29].

For the micro-milling fabrication, were used two approaches: optimized and non-optimized micro-milling. The optimizations were set up in ArtCam software. The optimized method used the parameters of the milling step equal to half of the tool diameter. In this study, the milling tool of 0.8 mm size was applied, therefore the milling step of 0.4 mm was used. While for the non-optimized micro-milling, the milling step was 0.8 mm. The optimized fabrication creates a smoother structure due to the low resolution of milling with a total fabrication process of more than 12 hrs. On the other hand, the not-optimized micro-milling resulted in a rough structure with a faster fabrication process around 6 hrs. The limitation of the long fabrication process for a single mold structure in micro-milling can be overcome by 3D printing, with comparable fabrication time to produce several structures simultaneously (up to six molds).

The 3D design from AutoCAD was exported into .stl files and printed using an SLA 3D printer (Formlabs, UK) with the smallest resolution setting of 25 μm. The SLA 3D printer was using a 1 L cartridge of resin (grey v4, Formlabs, UK). The printing orientation of the mold was 45° with full raft support (Fig. 1B). After the printing process, the mold structure was immersed in isopropyl alcohol (IPA) under an ultrasonic bath (Formlabs, UK) for 10 min, followed by resin curing (Formlabs, UK) at 65 °C, 1 hr under the ultraviolet light illumination. Next, the printed structures were stored in an oven at 65 °C for 8 hr. The fabricated molds both from micro-milling and 3D printing (Fig. 1 C and D) were then washed using DI water and IPA before the PDMS casting. 2.2. PDMS casting and microfluidic inspection

Polydimethylsiloxane (PDMS) elastomer (Dowsil™ 184 Silicone Elastomer, Dow Chemical, US) with a cured ratio solution of 10:1 were stirred and mixed (3 min, room temperature/R.T.). Next, the elastomer solution was degassed in the vacuum to remove the bubbles until the transparent color was achieved. Subsequently, the elastomer was cast into the mold, followed by baking in the oven (2 hrs, 65 °C). The hardened elastomer peeled off from the mold. A microscope slide with a size of 75 mm × 25 mm × 1 mm (Epredia™ Microscope Slides, Thermo Scientific, US) was cleaned in DI water and isopropyl alcohol (IPA) (Merck, USA) as a substrate. Both patterned elastomer surface and microscope slides were exposed under plasma O_2 (Expanded Plasma Cleaner PDC-002, Harrick Plasma, US) for 40 seconds. The patterned elastomer was flipped to the glass substrate and bonded with uniform pressure to all the surfaces. The microfluidic channel was functionalized using poly(dimethylsiloxane-b-ethylene oxide) (PDMS-b-PEO) as described in detail in [27]. A permanent magnet with a disc shape (d=15 mm, supermagnet, Webcraft GmbH, Germany) was positioned under the concentrated chamber to collect the labeled biomarkers before the MR sensor measurement.

For the flow test (Fig. 1E), 100 μL *(V_T)* of phosphate buffer (PB) was mixed with 2 μL of magnetic nanoparticles (MNPs) (d= 250 μm, Nanomag, Micromod, Germany).. The timer *(t)* is counted from the first drop and stops until the liquid reaches the outlet. The rest of the liquid in the inlet was pipetted and calculated for the rest of the volume *(Vi)*. The flow rate *(FR)* of the channel can be estimated by the following formula:

$$FR = \frac{V_T - V_i}{t} \quad (1)$$

For channel inspection and quality control (Fig. 2), the freshly peeled elastomer was sliced across the channel into thin pieces. Next, the sliced chips were attached to the microscope slide and inspected under the microscope (Wide-Field Upright, Nikon–Ni-E, Japan). Fig 2 depicted the channel heights from the casted elastomer from fabricated several molds.

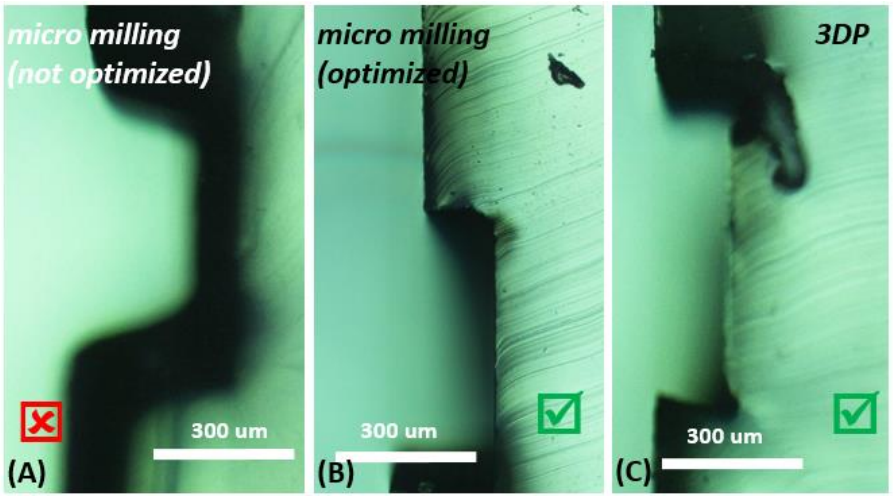

Figure 2. Inspection of the microfluidic channel from casted elastomer under a wide-field upright microscope. (A) Microfluidic chip from micro-milling mold (not optimized). It shows the channel height around 276 μm, which is not passed for quality control. Microfluidic chip, which passes quality control with a channel height ~150 μm; fabricated from the mold using (B) optimized micro-milling and (C) SLA 3D printing.

2.3 MNPs functionalization

2 μL of streptavidin-conjugated MNPs (d=250, concentration = 4.9×10^{11} mL^{-1}, Nanomag, Micromod) were incubated with 50 μg/mL of biotinylated polyclonal antibodies (Immunostep, Spain) of c-Fn or MMP9 during 1 hr. Next, the bovine serum albumin (BSA) (Sigma-Aldrich, Merck KGaA, Germany) 5% in phosphate buffer (PB) was used for MNP surface blocking in 1 h of incubation. Then, the MNPs for labeling c-Fn were diluted four times (1:4) and used undiluted (1:1) for MMP9. MNPs were mixed with serum-based matrices spiked with the interested biomarkers in the inlet microfluidic chip area in a total volume of 100 μL. The detail of MNP functionalization is reported elsewhere [29].

2.4. MR sensor and its functionalization

The MR biochip is composed of an array of 30 U-shaped spin-valve (SV) sensors and was microfabricated as reported previously [31–33]. The gold thin layer (12.9 × 35.4 μm²) above the SV sensors was treated with a heterobifunctional surface linker: 1 mg/mL of sulfosuccinimidyl 6-[3'-(2-pyridyldithio)propionamido] hexanoate (sulfo-LC-SPDP, Thermo Scientific, USA) in PB during 20 min. Then, 1 μL of monoclonal antibodies (Abcam, Cambridge, UK) at 250 μl/mL contacted with the sensor surface of 15 SV sensors for 2 h at room temperature (RT), followed by a blocking step with 1% of BSA. The remaining 15 SV sensors were used as negative control sensors and contacted with 5% of BSA.

2.5. Spiked biomarkers in human serum-based matrix

Human serum from male AB purchased from Sigma Aldrich (Merck, USA) was used untreated. Next, target proteins of c-Fn and MMP 9 were prepared at different concentrations around the clinical cutoff value of 3.4 µg/mL and 300 ng/mL, for c-Fn and MMP9, respectively (in a total volume of 100 uL of serum). Therefore, c-Fn was prepared in several concentrations of 1, 4, and 10 µg/mL; while MMP9 was prepared in concentrations of 100, 300, and 1000 ng/mL. In this work, it was used MNPs at a dilution ratio of 1:4 for c-Fn and undiluted for MMP9. Human serum samples spiked with the respective biomarkers were loaded into the microfluidic chip together with functionalized MNPs and followed the protocol described in [29].. The result of the labeling processing: MNP-labeled specific biomarkers were quantified at the MR biochip platform. The mechanism of the signal acquisition from the MR sensor is described in Fig. 3 (A and B). Briefly, a measurement is composed of three steps: (1) The baseline: is acquired by passing PB for 5 min over the MR sensor surfaces, which are immobilized with monoclonal antibodies (2) The saturation: MNPs complexes, i.e. MNP plus specific target captured by the microfluidic chip are inserted into the biosensor flowcell. After 5 mins, the magnetic focusing is applied to attract MNPs to the top of the MR sensor surface to distribute the MNPs uniformly and allow opportunities for monoclonal antibodies to capture the MNPs complexes. (3) The washing: after the saturation level of up to 25 min, the sensor surfaces are washed with PB-T (phosphate buffer with 0.05% Tween®20) until the signal is stable. In this step, most of the non-specific binding can be released from the sensor surface, remaining only specific binding. Finally, the differential signal between the baseline and saturation level after wash was recorded as the binding signal.

Figure 3. (A) An example of a binding signal measurement obtained for c-Fn using a portable MR biochip as a sensing element. (B) the sandwich assay strategy occurring at the gold surface of a MR sensor.

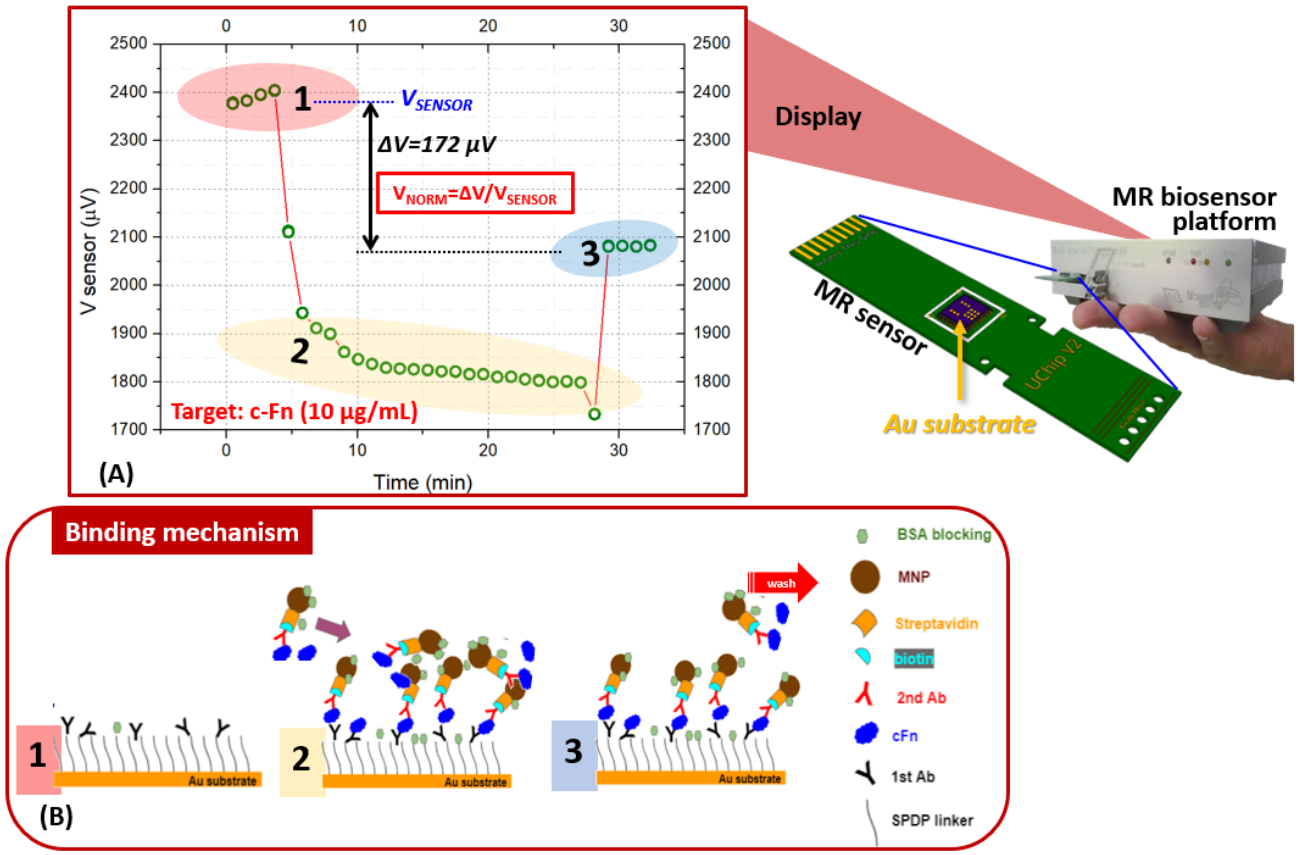

2.6. Statistical analysis

The MR composed of an array of 30 U-shaped SV sensors, where 15 were used for target binding, and the other 15 for negative control. The signals were collected from at least 10 sensors for target and negative control, respectively.

The measured voltage signal in each sensing area was normalized using the following formula:

$$V_{NORM} = \Delta V / V_{SENSOR} \quad (2)$$

Where V_{NORM} is the normalized signal value and unitless, ΔV is the delta between the average of the baseline and binding signal, and V_{SENSOR} is the average of the baseline (sensor output).

The average signals of active sensors in a measurement batch were calculated using the propagation of errors approach, where each average and standard deviation contribute to the calculated signal value. The curve fittings were obtained using the Hillsslope model, with a 95% confidence level of the calibration curve, using 1000 data points, ANOVA using a maximum of 400 iterations. The Signal level of detection limit (Y_{LOD}) was calculated using the formula from [35]:

$$Y_{LOD} = 1.645\ SD_{C0} + 1.645\ SD_{C1} \quad (3)$$

Where SD_{C0} and SD_{C1} are the standard deviations from blank measurement and smallest concentration, respectively.

3. Results and Discussion

3.1. Repeatability of the microfluidics

Molds fabricated by CNC and 3D printer were compared to a reference mold previously fabricated in other published work by CNC [29]. The parameters checked for the quality control (QC) of microfluidic chips produced from those different fabricated molds are summarized in Table 1. The molds with acceptable QC were used for PDMS casting to obtain the final microfluidic chips, which were tested against the interesting targets (c-Fn and MMP9). After the labeling on a chip, the levels of protein were quantified using an MR biochip platform to demonstrate the reproducibility of the molds, and respective repeatability of the measurements (Fig.4). The magnitude of the MR sensor signals is in a comparable range to the reference signal (light yellow region) obtained from our previous study[29]. In contrast, the microfluidic chips with higher channel thickness show that the signals were significantly lower than those that pass the QC.

Table 1. Inspection and quality control test: microfluidics chips from different fabricated molds.

	REFERENCE MOLD	CNC	OPTIMIZED CNC	3D PRINTER
Volume (serpentine + chamber)	25 μL	46 μL	25 μL	25 μL
Channel height	150 μm	276 μm	150 μm	150 μm
Quality Control	-	Failed	Passed	Passed

We provide in Fig.5 an illustration to explain the hypothesis behind the obtained results. The microfluidic with optimum channel height (Fig. 5A) shows a filtration mechanism by the MNPs cluster in the concentrated chamber. The MNPs clustered concentrated by the magnetic field from the permanent magnet capture the biomarkers that flow with

the sample medium. On the other hand, microfluidic chips with a higher channel height decreases the filtration efficiency of functionalized MNP clusters. The MNPs tend to be clustered in the substrate due to the magnetic field from the magnet, while the channel gap above potentially passes the biomarkers to the sponge. Moreover, the high channel heights enhanced the sponge absorption due to the increased surface contact with the medium. Although the idea of making the channel height as small as possible can lead to effective filtration, the longest absorption time is due to the light contact of the sponge surface with the medium.

Besides the channel height, we believe that other variables can also influence the effectiveness of the MNP filtration for the proposed microfluidic chip. First, the MNPs concentration is crucial to the dynamic range that can be tuned to fit the clinical cutoff value[27,28]. It is essential to get enough MNPs to cluster in the reaction chamber. Second is the preference of the magnet, i.e., the shape and the strength of the permanent magnet contribute to the filtration of the biomarkers. Weak magnetic fields may allow some functionalized MNPs to be absorbed into the sponge.

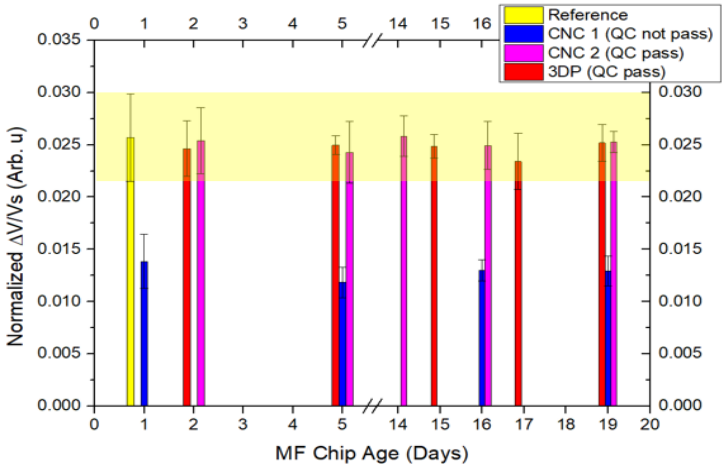

Figure 4. Reproducibility of the molds fabricated by micro-milling computer numerical control (CNC) and 3D printer (3DP), and respective repeatability of the measurements up to 19 days. The reference signal (yellow color) was referred from our previous work, and used here for comparison – such MF was obtained from a mold fabricated using CNC, and used for labeling c-Fn (10 µg/mL) in buffer[29].

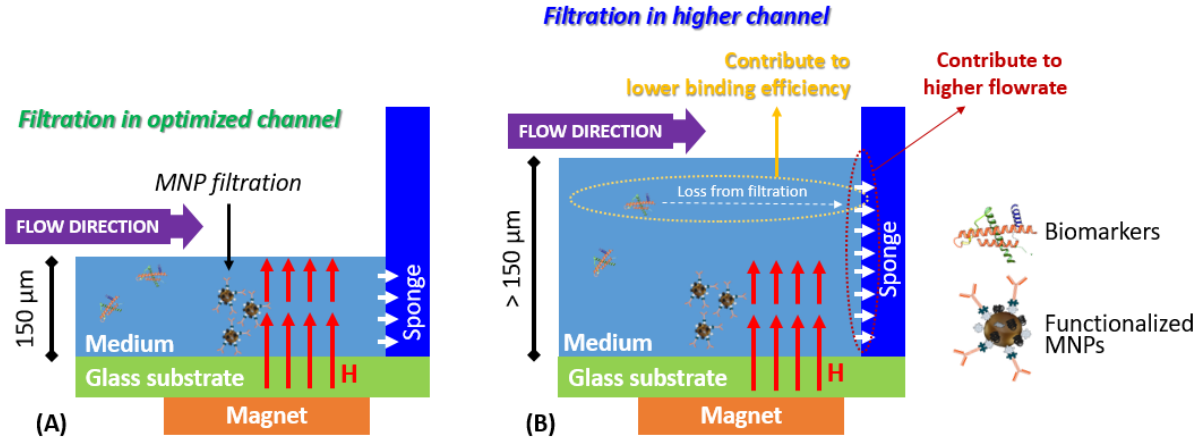

Figure 5. The critical role of the channel height of the microfluidic chip is to capture the target protein. (A) adequate protein labeling in an optimized channel. (B) A higher channel reduces the protein labeling efficiency and increases the contact surface of the medium with the sponges.

3.2. Protein labeling using human serum-based matrix

Stroke biomarkers were spiked in human serum-based matrices at the following concentrations: c-Fn at concentrations of 1, 4, and 10 µg/mL and MMP9 at concentrations of 100, 300, and 1000 ng/mL. These concentrations were prepared to understand if the technology (microfluidic chips and MR biochip platform) can be used to detect the biomarkers near the relevant clinical cutoff values defined for stroke patient stratification 3.4 µg/mL and 140ng/mL for c-Fn and MMP9, respectively[12,29]. To obtain the dynamic range that fit the clinical cutoff value, undiluted (1:1) and diluted (1:4) MNPs were used for the labeling of c-Fn and MMP9, respectively[29].

The quantification of c-Fn and MMP9 spiked in human serum is presented in Fig. 6 (A and B). The measurements obtained using a complex sample matrix (serum) were cross-validated against the measurements obtained in the proof-of-concept of the microfluidic device using biomarkers spiked in PB. The results showed that measurements performed using a complex sample matrix were in good agreement with the calibration curves of c-Fn and MMP9 labeled in the buffer. The standard deviation of the measurements obtained in serum, however, was slightly higher. The estimated limit-of-detection (LOD) were 205.14 ng/mL and 37.5 ng/mL for c-Fn and MMP9 in human serum-based matrix, respectively. These values are higher compared to the measurements obtained in a simple matrix: buffer, that were 54.6 ng/mL and 11.5 ng/mL for c-Fn and MMP9, respectively. This can be explained by the complex matrix of serum, derived from whole blood that contains several proteins that can increase the noise of biosensors and lead to non-specific binding events. It was reported that in human serum there are around 325 distinct proteins[35]. Albumin or immunoglobulins G are major proteins that can difficult the interaction between the specific antibodies attached to the MNPs and the interested biomarkers. Nevertheless, using the proposed microfluidic chip, the filtration mechanism described above (Fig. 5) by the MNPs occurs gradually, and it is sorted in a spotted area. It is utterly different from a conventional labeling method occurring in an Eppendorf™ tube that takes up to 1 hr (because of static incubation).

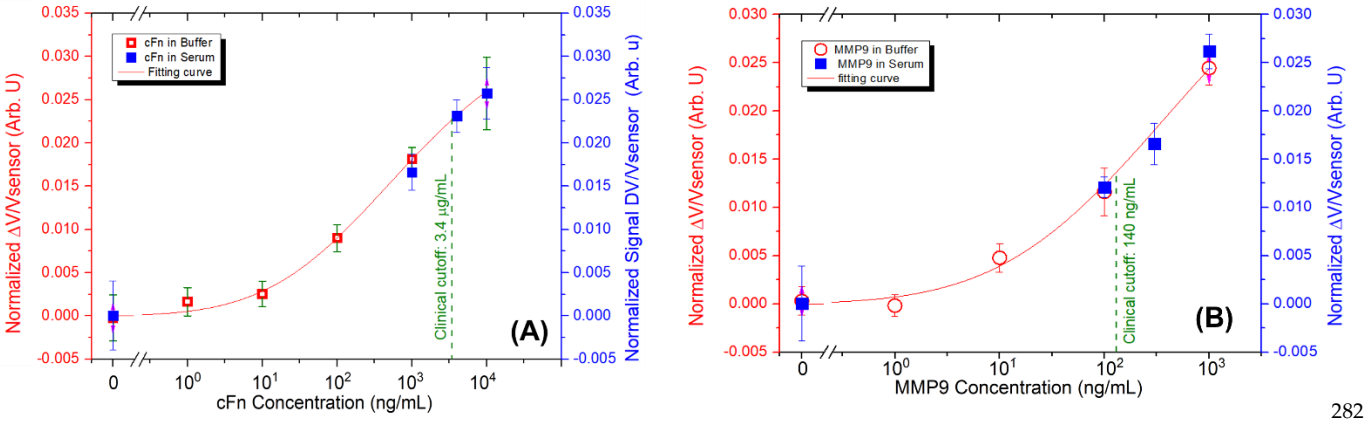

Figure 6. Quantification of c-Fn (A) and MMP9 (B) in human serum-based matrix (blue) near the relevant clinical cutoff regions. Measurements were cross-validated with the calibration curve obtained using biomarkers spiked in phosphate buffer (red). The green dash is the clinical cutoff value for each biomarker.

5. Conclusions

We have demonstrated a functional microfluidic chip for protein labeling in human serum. The microfluidic molds were fabricated using the micro-milling method and 3D printer, with optimized reproducibility for a channel height of 150 µm. The repeatability

of the microfluidic chips was successfully demonstrated by performing measurements using an MR biochip platform for several days – a proof-of-concept for quality control of the microfluidic chip production. The channel height plays the most crucial role in the labeling performance because of the magnetic field that exists from the bottom of the chip. The optimization of channel shapes and different pattern of magnetic fluxes are potentially explored for future work. Finally, the MNPs labeling of c-Fn and MMP9 in human serum can be performed in the proposed devices, with comparable performance for labeling the biomarkers in the buffer. The proposed method is feasible for the performance of clinical studies involving the tested biomarkers.

Author Contributions: Conceptualization, Briliant Adhi Prabowo; Elisabete Fernandes, Paulo Freitas; Data curation, Briliant Adhi Prabowo; Formal analysis, Briliant Adhi Prabowo and Elisabete Fernandes; Investigation, Briliant Adhi Prabowo and Elisabete Fernandes; Methodology, Briliant Adhi Prabowo and Elisabete Fernandes; Project administration, Elisabete Fernandes; Resources, Paulo Freitas; Supervision, Elisabete Fernandes, and Paulo Freitas; Validation, Carole Sousa Visualization, Briliant Adhi Prabowo; Writing – original draft, Briliant Adhi Prabowo Writing – review & editing, Carole Sousa and Elisabete Fernandes

Funding: This work was supported by FCT funding through project FIM4Stroke (reference PTDC/MEC-URG/29561/2017) **Acknowledgments:** The authors thank the micro and nanofabrication facilities of INL for the CNC and SLA 3D printer, and thanks to INESC-MN, Lisbon to provide the magnetoresistive sensors and readout platform.

Conflicts of Interest: The authors declare no conflict of interest.

References

1. Chou, Y. N.; Sun, F.; Hung, H. C.; Jain, P.; Sinclair, A.; Zhang, P.; Bai, T.; Chang, Y.; Wen, T. C.; Yu, Q.; Jiang, S. Ultra-low fouling and high antibody loading zwitterionic hydrogel coatings for sensing and detection in complex media. *Acta Biomater.* **2016**, *40*, 31–37, doi:10.1016/j.actbio.2016.04.023.
2. Warkiani, M. E. brahim.; Khoo, B. L. ua.; Wu, L.; Tay, A. K. a. P.; Bhagat, A. A. sga. S.; Han, J.; Lim, C. T., etc. Ultra-fast, label-free isolation of circulating tumor cells from blood using spiral microfluidics. *Nat. Protoc.* **2016**, *11*, 134–148, doi:10.1038/nprot.2016.003.
3. Garcia-Cordero, J. L.; Maerkl, S. J. Microfluidic systems for cancer diagnostics. *Curr. Opin. Biotechnol.* **2020**, *65*, 37–44, doi:10.1016/j.copbio.2019.11.022.
4. Taylor, A. B.; Zijlstra, P. Single-Molecule Plasmon Sensing: Current Status and Future Prospects. *ACS Sensors* **2017**, *2*, 1103–1122, doi:10.1021/acssensors.7b00382.
5. Ruiz-Vega, G.; García-Robaina, A.; Ben Ismail, M.; Pasamar, H.; García-Berrocoso, T.; Montaner, J.; Zourob, M.; Othmane, A.; del Campo, F. J.; Baldrich, E. Detection of plasma MMP-9 within minutes. Unveiling some of the clues to develop fast and simple electrochemical magneto-immunosensors. *Biosens. Bioelectron.* **2018**, *115*, 45–52, doi:10.1016/j.bios.2018.05.020.
6. Maestrini, I.; Ducroquet, A.; Moulin, S.; Leys, D.; Cordonnier, C.; Bordet, R. Blood biomarkers in the early stage of cerebral ischemia. *Rev. Neurol. (Paris).* **2016**, *172*, 198–219, doi:10.1016/j.neurol.2016.02.003.
7. Fernandes, E.; Sobrino, T.; Martins, V. C.; Lopez-loureiro, I.; Campos, F.; Germano, J.; Rodríguez-Pérez, M.; Cardoso, S.; Petrovykh, D. Y.; Castillo, J.; Freitas, P. P. Point-of-care quantification of serum cellular fibronectin levels for stratification of ischemic stroke patients. *Nanomedicine Nanotechnology, Biol. Med.* **2020**, *30*, 102287, doi:10.1016/j.nano.2020.102287.
8. Misra, S.; Kumar, A.; Kumar, P.; Yadav, A. K.; Mohania, D.; Pandit, A. K.; Prasad, K.; Vibha, D. Blood-based protein biomarkers for stroke differentiation: A systematic review. *Proteomics - Clin. Appl.* **2017**, *11*, 9–10, doi:10.1002/prca.201700007.
9. Rodríguez-Yáñez, M.; Sobrino, T.; Arias, S.; Vázquez-Herrero, F.; Brea, D.; Blanco, M.; Leira, R.; Castellanos, M.; Serena, J.; Vivancos, J.; Dávalos, A.; Castillo, J. Early biomarkers of clinical-diffusion mismatch in acute ischemic stroke. *Stroke* **2011**, *42*, 2813–2818, doi:10.1161/STROKEAHA.111.614503.
10. NCBI MMP9 matrix metallopeptidase 9 [Homo sapiens (human)] Available online:

https://www.ncbi.nlm.nih.gov/gene/4318 (accessed on Jun 1, 2021).

11. Wang, L.; Deng, L.; Yuan, R.; Liu, J.; Li, Y.; Liu, M. Association of Matrix Metalloproteinase 9 and Cellular Fibronectin and Outcome in Acute Ischemic Stroke: A Systematic Review and Meta-Analysis. *Front. Neurol.* **2020**, *11*, 1–11, doi:10.3389/fneur.2020.523506.
12. Castellanos, M.; Sobrino, T.; Millán, M.; García, M.; Arenillas, J.; Nombela, F.; Brea, D.; Perez De La Ossa, N.; Serena, J.; Vivancos, J.; Castillo, J.; Dávalos, A. Serum cellular fibronectin and matrix metalloproteinase-9 as screening biomarkers for the prediction of parenchymal hematoma after thrombolytic therapy in acute ischemic stroke: A multicenter confirmatory study. *Stroke* **2007**, *38*, doi:10.1161/STROKEAHA.106.481556.
13. Karabacak, N. M.; Spuhler, P. S.; Fachin, F.; Lim, E. J.; Pai, V.; Ozkumur, E.; Martel, J. M.; Kojic, N.; Smith, K.; Chen, P. I.; Yang, J.; Hwang, H.; Morgan, B.; Trautwein, J.; Barber, T. A.; Stott, S. L.; Maheswaran, S.; Kapur, R.; Haber, D. A.; Toner, M. Microfluidic, marker-free isolation of circulating tumor cells from blood samples. *Nat. Protoc.* **2014**, *9*, 694–710, doi:10.1038/nprot.2014.044.
14. Tai, W.-C.; Chang, Y.-C.; Chou, D.; Fu, L.-M. Lab-on-Paper Devices for Diagnosis of Human Diseases Using Urine Samples—A Review. *Biosensors* **2021**, *11*, 260, doi:10.3390/bios11080260.
15. Au, S. H.; Storey, B. D.; Moore, J. C.; Tang, Q.; Chen, Y. L.; Javaid, S.; Sarioglu, A. F.; Sullivan, R.; Madden, M. W.; O'Keefe, R.; Haber, D. A.; Maheswaran, S.; Langenau, D. M.; Stott, S. L.; Toner, M. Clusters of circulating tumor cells traverse capillary-sized vessels. *Proc. Natl. Acad. Sci. U. S. A.* **2016**, *113*, 4947–4952, doi:10.1073/pnas.1524448113.
16. Tan, W.; Powles, E.; Zhang, L.; Shen, W. Go with the capillary flow. Simple thread-based microfluidics. *Sensors Actuators, B Chem.* **2021**, *334*, doi:10.1016/j.snb.2021.129670.
17. Zuo, Z.-Q.; Pan, J.-Z.; Fang, Q. An integrated microfluidic system for multi-target biochemical analysis of a single drop of blood. *Talanta* **2022**, *249*, 123585, doi:10.1016/j.talanta.2022.123585.
18. Almughamsi, H. M.; Howell, M. K.; Parry, S. R.; Esene, J. E.; Nielsen, J. B.; Nordin, G. P.; Woolley, A. T. Immunoaffinity monoliths for multiplexed extraction of preterm birth biomarkers from human blood serum in 3D printed microfluidic devices. *Analyst* **2022**, *147*, 734–743, doi:10.1039/d1an01365c.
19. Malhotra, B. D.; Ali, M. A. *Microfluidic Biosensor*; 2018; ISBN 9780323449236.
20. Kim, T.; Yi, Q.; Hoang, E.; Esfandyarpour, R. A 3D Printed Wearable Bioelectronic Patch for Multi-Sensing and In Situ Sweat Electrolyte Monitoring. *Adv. Mater. Technol.* **2021**, *6*, 1–11, doi:10.1002/admt.202001021.
21. Guckenberger, D. J.; De Groot, T. E.; Wan, A. M. D.; Beebe, D. J.; Young, E. W. K. Micromilling: A method for ultra-rapid prototyping of plastic microfluidic devices. *Lab Chip* **2015**, *15*, 2364–2378, doi:10.1039/c5lc00234f.
22. Cong, H.; Zhang, N. Perspectives in translating microfluidic devices from laboratory prototyping into scale-up production. *Biomicrofluidics* **2022**, *16*, doi:10.1063/5.0079045.
23. Del Giudice, F.; Madadi, H.; Villone, M. M.; D'Avino, G.; Cusano, A. M.; Vecchione, R.; Ventre, M.; Maffettone, P. L.; Netti, P. A. Magnetophoresis "meets" viscoelasticity: Deterministic separation of magnetic particles in a modular microfluidic device. *Lab Chip* **2015**, *15*, 1912–1922, doi:10.1039/c5lc00106d.
24. Mesquita, P.; Gong, L.; Lin, Y. A Low-Cost Microfluidic Method for Microplastics Identification: Towards Continuous Recognition. *Micromachines* **2022**, *13*, 499, doi:10.3390/mi13040499.
25. Gonzalez, G.; Roppolo, I.; Pirri, C. F.; Chiappone, A. Current and emerging trends in polymeric 3D printed microfluidic devices. *Addit. Manuf.* **2022**, *55*, 102867, doi:10.1016/j.addma.2022.102867.
26. Stefano, J. S.; Guterres e Silva, L. R.; Rocha, R. G.; Brazaca, L. C.; Richter, E. M.; Abarza Muñoz, R. A.; Janegitz, B. C. New conductive filament ready-to-use for 3D-printing electrochemical (bio)sensors: Towards the detection of SARS-CoV-2. *Anal. Chim. Acta* **2022**, *1191*, doi:10.1016/j.aca.2021.339372.
27. Fei, G.; Nie, L.; Zhong, L.; Shi, Q.; Hu, K.; Parra-Cabrera, C.; Oprins, H.; Ameloot, R.; Yang, S. Photocurable resin-silica

composites with low thermal expansion for 3D printing microfluidic components onto printed circuit boards. *Mater. Today Commun.* **2022**, *31*, 103482, doi:10.1016/j.mtcomm.2022.103482.

28. Namgung, H.; Kaba, A. M.; Oh, H.; Jeon, H.; Yoon, J.; Lee, H.; Kim, D. Quantitative Determination of 3D-Printing and Surface-Treatment Conditions for Direct-Printed Microfluidic Devices. *Biochip J.* **2022**, *16*, 82–98, doi:10.1007/s13206-022-00048-1.
29. Prabowo, B. A.; Fernandes, E.; Freitas, P. A pump-free microfluidic device for fast magnetic labeling of ischemic stroke biomarkers. *Anal. Bioanal. Chem.* **2022**, *414*, 2571–2583, doi:10.1007/s00216-022-03915-w.
30. Maestrini, I., Ducroquet, A., Moulin, S., Leys, D., Cordonnier, C., Bordet, R. Blood biomarkers in the early stage of cerebral ischemia. Rev. Neurol. (Paris). 2016, 172, 198–219. https://doi.org/10.1016/j.neurol.2016.02.003
31. Martins, V. C.; Cardoso, F. A.; Germano, J.; Cardoso, S.; Sousa, L.; Piedade, M.; Freitas, P. P.; Fonseca, L. P. Femtomolar limit of detection with a magnetoresistive biochip. *Biosens. Bioelectron.* **2009**, *24*, 2690–2695, doi:10.1016/j.bios.2009.01.040.
32. Marquina, C.; De Teresa, J. M.; Serrate, D.; Marzo, J.; Cardoso, F. A.; Saurel, D.; Cardoso, S.; Freitas, P. P.; Ibarra, M. R. GMR sensors and magnetic nanoparticles for immuno-chromatographic assays. *J. Magn. Magn. Mater.* **2012**, *324*, 3495–3498, doi:10.1016/j.jmmm.2012.02.074.
33. Freitas, P. P.; Cardoso, F. A.; Martins, V. C.; Martins, S. A. M.; Loureiro, J.; Amaral, J.; Chaves, R. C.; Cardoso, S.; Fonseca, L. P.; Sebastião, A. M.; Pannetier-Lecoeur, M.; Fermon, C. Spintronic platforms for biomedical applications. *Lab Chip* 2012, *12*.
34. Armbruster, D. A.; Pry, T. Limit of blank, limit of detection and limit of quantitation. *Clin. Biochem. Rev.* **2008**, *29 Suppl 1*, S49-52.
35. Pieper, R.; Gatlin, C. L.; Makusky, A. J.; Russo, P. S.; Schatz, C. R.; Miller, S. S.; Su, Q.; McGrath, A. M.; Estock, M. A.; Parmar, P. P.; Zhao, M.; Huang, S.-T.; Zhou, J.; Wang, F.; Esquer-Blasco, R.; Anderson, N. L.; Taylor, J.; Steiner, S. The human serum proteome: Display of nearly 3700 chromatographically separated protein spots on two-dimensional electrophoresis gels and identification of 325 distinct proteins. *Proteomics* **2003**, *3*, 1345–1364, doi:https://doi.org/10.1002/pmic.200300449.